Research Article

Xiaoning Zhao, Daqing Wang*, Haoli Xu, Yue Shi, Zhengdong Deng, Zhibin Ding, Zhixin Liu, Xingang Xu, Zhao Lu, Guangyuan Wang, and Zijian Cheng

Water deep mapping from HJ-1B satellite data by a deep network model in the sea area of Pearl River Estuary, China

https://doi.org/10.1515/geo-2020-0267
received October 21, 2020; accepted June 04, 2021

Abstract: Remote sensing (RS) water depth inversion is an important technology and the method of water depth measurement. Taking the waters around the islands outside the Pearl River Estuary as an example, five optical RS depth inversion algorithms were introduced. Then, five water depth inversion models were trained through the HJ-1B satellite RS image and the measured water depth data. The results show that the mean absolute error (MAE) of the deep learning model was the smallest (2.350 m), and that the distribution of predicted water depth points was closest to the actual value. Deep learning has been widely used in RS image classification and recognition and shows its advantages. Therefore, the deep learning model was applied to extract the depth of the shallow water. Meanwhile, the obtained inversion effect map is closest to the actual contour map. The water depth inversion performance of back propagation neural network model is better than that of the radial basis function (RBF) neural network model. Besides, the inversion accuracy of the RBF neural network may be affected due to the small amount of data and the improper number of hidden neurons. The results show broad application prospects of machine learning algorithms in RS water depth inversion. Also, this study provided data support for model optimization, training, and parameter setting.

* **Corresponding author: Daqing Wang,** Defense Engineering College, Army Engineering University, Nanjing, Jiangsu 210007, China, e-mail: wangdq_cumt@sina.com
Xiaoning Zhao, Haoli Xu, Yue Shi, Zhengdong Deng, Zhibin Ding, Zhao Lu, Guangyuan Wang, Zijian Cheng: Defense Engineering College, Army Engineering University, Nanjing, Jiangsu 210007, China
Zhixin Liu, Xingang Xu: School of Resources and Geosciences, China University of Mining and Technology, Xuzhou, Jiangsu 221116, China

Keywords: RS, HJ-1B, water depth inversion, deep learning

1 Introduction

The ocean plays a vital role in the strategic layout of national security and economical construction, and the water depth is the essential marine element in shallow seas. Whether in the construction of ports, docks, waterways, and anchorages, or in the safe navigation of ships, marine scientific research, marine engineering construction, and marine environmental assessment need the water depth data as the primary guarantee [1]. Traditional water depth measurement methods have large limitations and take a long time. The water depth remote sensing (RS) technology is favored because of its wide range and short-time consumptions.

Solar radiation is weakened by the atmosphere (absorption, reflection, and scattering) before reaching the surface of the water body, and only few part of the energy is reflected to the atmosphere at the water–air interface. The main energy enters the water body through water surface refraction [1]. By collecting the optical radiation information received by the sensor and performing preprocessing operations such as atmospheric correction, this study obtained some information. The information included the spectral information and the water body bottom and topography information contained in the water emission and reflection spectra of the study area. Then, the study used the water depth inversion model to invert the study area [2]. Since the 1970s, with the formation and development of RS satellite technology, the water depth RS inversion method has been known by researchers because of its unique advantages. Then, various water depth inversion models have been continuously proposed [3]. According to the principle of water depth optical inversion by RS, the methods of deriving the water depth inversion model based on the

relationship between the water depth and the reflection spectrum are called the density method. The density methods were divided into three categories [4] according to the different calculation methods.

The theoretical interpretation model was derived from the radiation transmission model. The advantage of the model is that the inversion results are more accurate. The disadvantage is that the inversion process must have a certain amount of optical parameter data as a support. But the amount of the optical parameter data that the inversion process requires is so large that the model is not easy to implement, the equations are challenging to solve, and the application in the inversion process is less. Only by making the theoretical interpretation model more perfect [5], it can be more convenient for water depth inversion [6]. Polcyn et al. simplified the theoretical interpretation model by using the research of Polcyn as a basis, making it possible to apply this model to actual water depth back evolution [7].

The semi-theoretical and semi-empirical model combined theoretical interpretation models and empirical algorithms, and performed regression analysis through measured parameter data to obtain the correlation between reflectivity and water depth, and then inverted the water depth of the entire area. The theoretical interpretation model required a small number of parameters and only required that the input optical radiation data of the local water body can be used to derive the global water depth inversion results, and the inversion accuracy was better. According to the attenuation curve of the reflection spectrum of sunlight passing through water bodies at different depths, Benny and Dawson developed a single-band model (only for single-band water depth inversion) and verified its feasibility [8]. John et al. proposed a multiband water depth inversion model based on a constant ratio of the bottom water reflectivity between bands, ignoring the influence of the water substrate on the reflection spectrum. Besides, the accuracy of the inversion was verified [9]. Jingjing and Qingjiu proposed to use the B3 and B4 bands of Landsat 8 data to construct a band ratio water depth inversion model and used the inversion results to draw a water depth map [10]. After processing the water depth of Hongze Lake, the average water depth error of the inversion value was 0.35 m, and the effect was better. The assumptions of the aforementioned two models were also to ignore the influence of the bottom of the water body, so as far as possible the interference of low environmental noise and other factors on water depth inversion, with high inversion accuracy and good effect [11]. Benqing et al. applied domestic GF-1 satellite data to carry out image geometric correction, atmospheric correction, and flare correction preprocessing. Based on the dual-band water depth inversion model and the logarithmic ratio model, the water depth inversion of Jinsha Island in Xisha Islands was performed by RS, and the measured data was used to prove the Jinqing Island GF-1 satellite data based on the dual-band linear model. Water depth inversion results were significantly better than the dual-band logarithmic ratio model [12].

The statistical model is based on statistical ideas and methods. The data objects are as follows: sunlight radiating on the water surface, water body-atmospheric scattering, and water body bottom reflection, to establish the relationship between the measured area water depth value and the RS optical image spectrum. Knowing the linear relationship, the correlation of these can be used to infer the water depth value. The method was mature and widely used in water depth inversion. Based on the different types of functions used in the model, the statistical model can be divided into linear function model [13], logarithmic function model [14], exponential function model [15], power exponential function model [16], quadratic polynomial function model, and so on.

The introduction of multiple bands further weakened the interference of different substrates on light reflectance. Water depth was independent of the substrate type. During the inversion process, regression analysis was performed on the measured water depth data to calculate relevant parameters. Most of the models described earlier were based on the correlation between the optical signal's bottom reflection spectrum information and the water depth. Therefore, the limitations of the aforementioned models were also undeniable [17]. After nearly 50 years of research, optical water depth inversion models have been continuously developed and gradually overcome. The following research introduced new methods into water depth inversion to overcome the problems existing in the previous model. Sandidge and Holyer introduced machine learning to water depth inversion, combining the neural network method with water depth RS inversion for the first time. Then Sandidge and Holyer used the water hyperspectral data and measured the water depth data of the study area to establish a neural network multilevel decision-making water depth inversion [18].

In recent years, on the basis of actual situation of the research area, scholars have constantly adjusted the neural network model to adapt to the inversion of water depth in more complex waters. In the water depth inversion of the Yangtze estuary, Wang introduced the "suspended sediment influence factor" based on the neural

network model, which improved the accuracy of the neural network model in the inversion of the turbid water depth [19]. Zhicheng introduced chlorophyll and sediment into the neural network model to retrieve the depth of Dalian Bay [20]. Hongqi et al. proposed a modeling method that introduced support vector machine (SVM) into water depth inversion, constructed a SVM inversion model, and proved the potential of this model in water depth inversion [21]. Xu applied neural network technology to the domestic HJ-1A satellite for shallow water depth inversion and realized the application of HJ-1A satellite in shallow water depth inversion [22]. Yanguo and Jinxia compared the water depth inversion capability of the traditional linear model and the neural network model and proved the advantages of the neural network model in dealing with the water depth inversion problem in terms of the model's adaptive ability and mapping ability [23]. Subsequently, Bin et al. added particle swarm algorithm to train the water depth data in the process of inverting the water depth of the neural network model, improving the iterative convergence speed of the neural network model. Bin et al. also proved that the improved algorithm was better than the traditional neural network algorithm in the depth of water depth of 30 m or less [24]. Guizhou et al. compared the back propagation (BP) and radial basis function (RBF) neural network models. They changed the parameters of the BP network through the control variable method to maximize the correlation coefficient of training. The trained BP and RBF networks were applied to the water depth inversion of Mischief Reef, and the advantages and disadvantages of the two neural networks were analyzed from different angles [25].

So far, domestic and foreign scholars had established a variety of models of RS depth inversion for different data sources and research areas and achieved good results. However, it had to be admitted that the technology of RS depth inversion was not perfect, and its accuracy and stability cannot yet replace traditional measurement methods. As a machine learning algorithm that was closer to artificial intelligence, deep learning had achieved image recognition results. These results were far exceeding the results that were achieved by previous related technologies [26]. This study attempted to combine deep learning algorithms with RS water depth inversion to explore a more accurate model.

2 Data

This section introduced the study area and the RS satellite data. The characteristics of the study area and the characteristics of the HJ-B satellite data were explained.

2.1 The overview of the study area

The sea area of the archipelago outside the Pearl River Estuary has geographical coordinates between 113°37E and 114°21E and between 21°44 N and 22°12 N (Figure 1). The maximum length of the studied area is 30 km, the maximum width is 45 km, and the average water depth is about 30 m. It has a subtropical maritime climate, with sufficient sunshine and abundant rain.

The Islands off the Pearl River Estuary, located outside the Pearl River Estuary in Guangdong Province, is the second largest archipelago after Zhoushan Islands in China. It consists of more than 150 islands. The larger ones are Hong Kong Island, Datong Island, Hengqin Island,

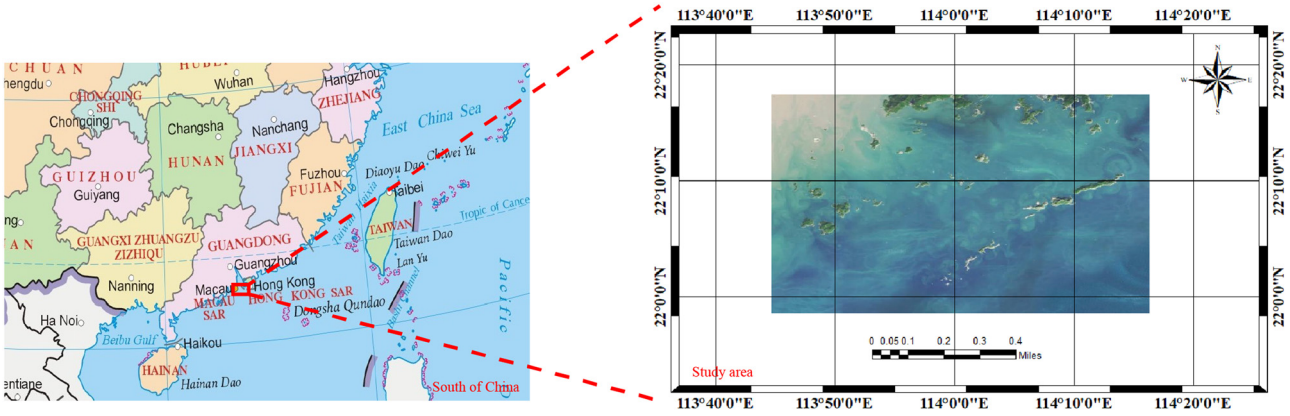

Figure 1: The map of the study area.

Gaolan Island, Hebao Island, Dajin Island, Shangchuan Island, and Xiachuan Island, and the smaller islands include Wanshan Islands, Po Toi Islands, and Dangan Islands. They are administratively divided into Hong Kong, Macau, Zhuhai city, and Taishan county. Because it is affected by the North-East-South-West fault, it is arranged in a series of northeast directions, surrounded by the Pearl River Funnel Bay mouth, and stretches over 160 km. The archipelago was originally a continental mountain range (Lotus mountain) and later separated from the mainland into islands due to mountain subsidence and seawater intrusion.

The archipelago waters are good fishing grounds, and the Pearl River estuary, which is the place for fish to feed and spawn, is rich in bait. Besides, the fishing industry is pretty developed. In terms of transportation, there are highways on the island, beacon for Guangzhou and Hong Kong route navigation target. Due to its excellent geographical location, the archipelago has been a gateway for foreign trade and traffic, especially Hong Kong Island. Hong Kong Island is the world's leading waterway and the largest trading port in the East. Wanshan archipelago is the only way for Guangzhou to voyage to sea, which is located at the mouth of the Pearl River and under the jurisdiction of Zhuhai City.

2.2 Overview of HJ-1B satellite data

China's "environment and disaster monitoring small satellites" A and B (HJ-1A and HJ-1B) were launched in Taiyuan Satellite Launch Center on September 6, 2008. It is the first small satellite constellation dedicated to the environment and disaster monitoring and prediction in China and is another new civil satellite system launched after the meteorological, marine, and resource satellite series in China. HJ-1B is a sun synchronous orbit near noon, with an orbit height of about 650 km. It carries two widecover multispectrum cameras and an infrared sensor, with a revisit period of about 96 h. The CCD camera has a width of 360 km, the combined width of the two sets is greater than 700 km, and the spectrum range is 0.43–0.9 μm. The resulting image is divided into four bands with a resolution of 30 m under the satellite. The infrared scanner has a width of 720 km, the spectral range is 0.75–12.5 μm, and the obtained image is also divided into four bands. Subsatellite point resolution of the first three bands (near infrared, short wave infrared, and mid infrared) is 150 m, and Subsatellite point resolution of the fourth band (thermal infrared (band)) is 300 m [27]. HJ-1B satellite's wide observation width and other characteristics can provide strong support for large-scale, all-weather dynamic monitoring of the environment.

3 The introduction of methods

The methods used in this study included deep learning, curve fitting, and simple machine learning algorithms. The calculation principle of each algorithm was different, and the characteristics of different algorithms were explained in detail.

3.1 Deep learning method

The concept of deep learning comes from the study of the artificial neural network. A multilayer sensor with multiple hidden layers is a deep learning structure. Deep learning can combine low-level features and then build more comprehensive high-level attribute features layer by layer. Deep learning model has five to ten layers or more neural networks, while traditional neural networks usually have only two or three layers. Moreover, the parameters and computing nodes of traditional neural network are limited, and its ability to learn and express complex functions is limited. The complex structure of deep learning makes it to produce more effective training mechanism. The hierarchical structure of deep learning model is only connected between adjacent layers of neurons, and the same layer and cross layer neurons are not connected with each other, which is similar to the structure of human brain, and can imitate the brain to express information efficiently and accurately [28].

3.2 Curve fitting methods

Curve fitting uses a certain model to fit a series of data into a smooth curve, to observe the internal relationship between the data and the model, and to understand the changing trend of the data. Commonly used models include linear model, polynomial model, exponential model, and Gaussian model. Generally, the model used can be determined according to the characteristics of the specialty. When the model cannot be determined, the scatter diagram can be drawn, and the appropriate curve type can be selected according to the distribution of the scatter [29].

3.3 BP neural network

The BP neural network is a kind of multilayer feed forward neural network. Its main feature is that it can forward to transmit the signal and back transmit the error [30]. It uses the error after output to estimate the error of the direct leading layer of the output layer and then uses this error to estimate the error of the previous layer, so that the error estimation of all other layers can be obtained if the layer passes backward, and the connection weight of the network can be constantly changed by the obtained error, so as to make the output of the network keep close to the expected output (Figure 2).

3.4 RBF neural network

RBF neural network is a three-layer neural network, which includes input layer, hidden layer, and output layer. Both the RBF neural network and the BP neural network belong to the feedforward neural network. Different from the BP neural network, the transformation from input space to hidden layer space of the RBF neural network is nonlinear, while the transformation from hidden space to output space is linear. In other words, RBF is used as the "base" of the hidden unit to form the hidden layer space. In this way, the input vector can be directly mapped to the hidden space without weight connection. When the center point of RBF is determined, the mapping relationship is determined. The mapping from the hidden layer space to the output space is linear, that is, the output of the network is the linear weighted sum of the output of the hidden unit, and the weight here is the adjustable parameter of the network. Among them, the function of the hidden layer is to map vector from low dimension to high dimension, so that low-dimension linear indivisibility can become linear separable from high dimension. In this way, the mapping from input to output of the network is nonlinear, while the output of the network is linear to the adjustable parameters. The weight of the network can be directly solved by the linear equations, thus speeding up the learning speed and avoiding the local minimum problem [32].

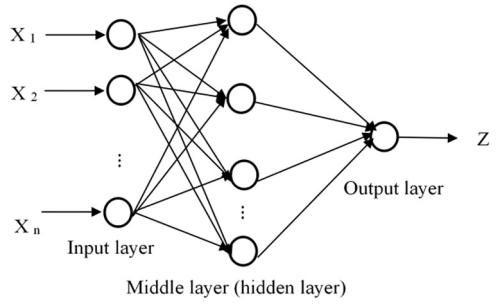

Figure 2: The simple structure of the BP neural network [31].

3.5 SVM neural network

SVM was first proposed by Cortes and Vapnik. It is a supervised learning model and related learning algorithm to analyze data in classification and regression analysis. The main idea of SVM is to build a classification hyperplane as the decision surface, so that the isolation edge between positive and negative examples is maximized [33].

When the data are linearly separable, the linear classifier can be learned by maximizing the hard interval, that is, the hard interval SVM; when the training data is not linearly separable but nearly linearly separable, the linear classifier can also be learned by maximizing the soft interval, that is, the soft interval SVM; when the training data are linearly separable, it can be learn by maximizing the inner product kernel and the soft interval. A nonlinear SVM is obtained. Therefore, SVM can provide good generalization performance in pattern classification, which is unique to SVM.

4 Applications and results of different methods

The water depth data are divided into the training set and the test set. The training set was used to train each model, and the test set was imported into the trained model to obtain the depth inversion results of different methods.

4.1 The results of deep learning

This study used a deep feed forward neural network (DFNN). In the regression task, it can extract advanced features from a large number of variables to obtain high prediction accuracy. This study used keras's deep learning framework to build the DFNN model. The specific training process of deep learning includes feature learning using bottom-up and unsupervised methods. First, the first layer was trained without calibration data to learn the parameters of itself. Due to the large capacity and loose

Table 1: A selection of results of tuning the key parameters of the model

Hidden layers	Neurons	Epochs	Train R^2	Train MAE	Test R^2	Test MAE
3	36	50	0.627	1.471	0.601	5.936
3	36	100	0.711	0.684	0.697	3.215
3	36	150	0.764	0.602	0.722	3.154
4	36	50	0.890	0.123	0.825	2.350
4	36	100	0.832	0.101	0.825	2.946
4	36	150	0.816	0.166	0.790	3.054
5	36	50	0.894	0.094	0.791	3.468
5	36	100	0.887	0.167	0.727	3.271
5	36	150	0.845	0.085	0.704	3.240
...	...	...	...	...	...	...

constraints of the model, the generated model can learn from the data structure itself and obtain more features than the input. After learning to obtain the N-1 layer, the output of the N-1 layer was taken as the input of the N-layer, and the N-layer was trained, thereby obtaining the parameters for each layer. In addition, the model adopted top-down supervised learning. By using labeled data for training, the error propagated backward in order, and the weight of each layer was adjusted.

The training set and the test set were used to find the optimal parameters of the model. The correlation coefficient (R^2) and MAE of the model were obtained by adjusting the number of hidden layers, neurons, and epochs. The selection of the results is presented in Table 1. When the maximum R^2 and minimum MAE of the training set appeared, the R^2 and MAE of the test set were not optimal. This result showed that the blindly pursuing of minimizing the error of training set may lead to the decline of the ability to predict unknown data (test set). Therefore, to avoid overfitting and improve the generalization ability of the model, it was important to consider the evaluation parameters of training set and test set at the same time. In this study, the following were finally selected as the initial input parameters of the model: hidden layers = 4, neurons = 36, and epochs = 50. As presented in Table 1, R^2 between the predicted depth and the measured value of the training set was 0.890, and the R^2 between the predicted depth and the measured value of the test set was 0.825. In addition, the MAE of training set and test set were 0.123 and 2.350, respectively. The result showed that the simulation accuracy of the model is high, and the prediction ability of new data was also improved.

The prediction result of this deep network structure is shown in Figure 3.

4.2 The results of curve fitting models

Considering the different indexes (some bands) had different correlation coefficient with the values of water

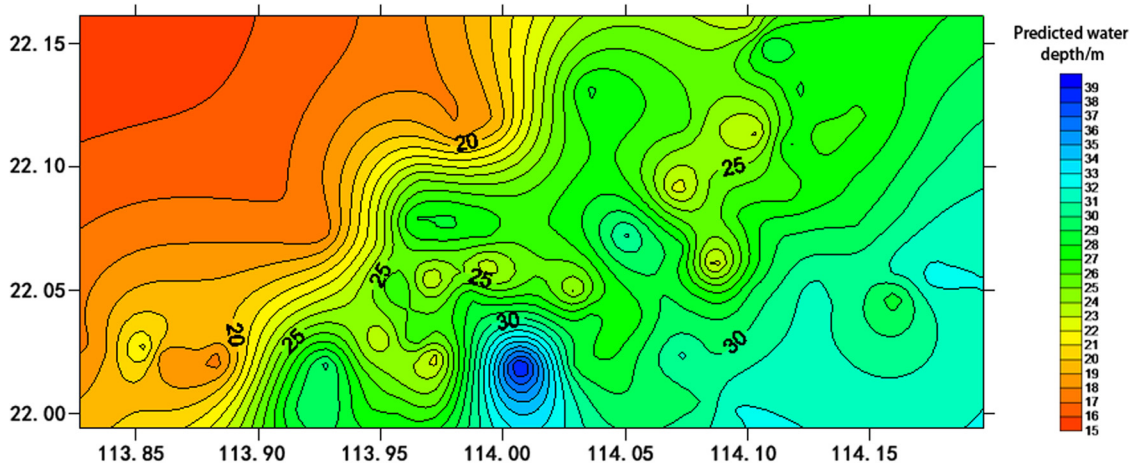

Figure 3: Prediction results of water depth based on deep learning model.

Table 2: The correlation coefficient between different indexes (some bands) and water depth in this area

Correlation coefficient	Inversion indexes										
	B1	B2	B3	B4	B1/B2	B2/B3	B3/B2	B1/B3	B1/B4	B4/B1	B2/B4
ρ	0.764	0.696	0.393	−0.661	−0.387	0.600	−0.635	0.606	0.776	−0.808	0.704

deep in this area, the study referred to some researches [23,32] and did a correlation analysis, which is presented in Table 2.

According to Table 2, the correlation coefficient between B4/B1 band ratio and water depth in this area was the highest. Therefore, the band ratio of B4/B1 was selected as the input value for the inversion of water depth in this area by the curve fitting model (Figure 4).

According to Table 3, the cubic model had the better results than other curve fitting models with the lower R, R^2, and so on ($R = 0.875$, $R^2 = 0.766$, R^2 (modified) = 0.761, and the standard error of the estimate = 0.353). Thus, the study wound use the cubic model to inverse the water deep value of the area. The inversion result is shown in Figure 5.

4.3 The results of BP neural network

In this study, 60% of the total data and 40% of the total data were used as the training set and the test set. The structure of the BP neural network is shown in Figure 6. The B1–B4 and B4/B1 band data were used as the input of the model.

The MAE of training results was 1.674, and the standard deviation was 2.194; the MAE of test results was 2.455, and the standard deviation was 3.271. The importance of predictive variables of the model was 0.35, 0.25, 0.21, 0.11, and 0.09 (B4/B1, B4, B2, B3, B1, respectively). The inversion result is shown in Figure 7.

4.4 The results of RBF neural network

In this study, 60% of the total data and 40% of the total data were used as the training set and test set. The structure of the RBF neural network is shown in Figure 8. The B1–B4 and B4/B1 band data were used as the input of the model.

The MAE of training results was 1.838, and the standard deviation was 2.47; the MAE of test results was 2.719, and the standard deviation was 3.702. The importance of predictive variables of the model was 0.25, 0.25, 0.25, 0.17, and 0.08 (B4/B1, B2, B1, B4, and B3, respectively). The prediction result is shown in Figure 9.

4.5 The results of SVM

This study used SVM with a linear function kernel. The training set and the test set were composed of 60% of the

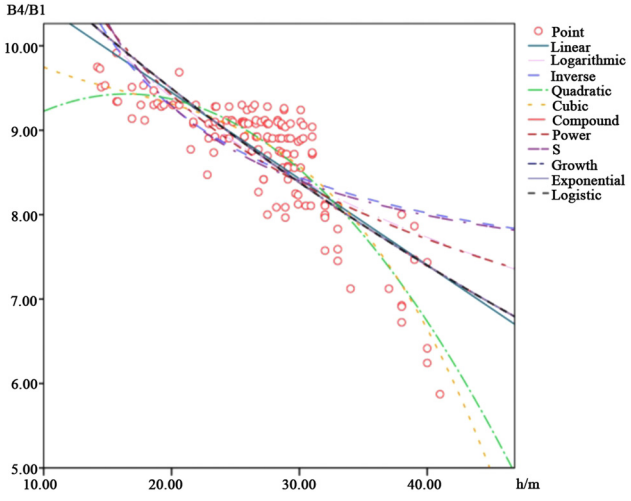

Figure 4: The results of curve fitting models of water deep in this study area.

Table 3: The results of curve fitting

Names of models	R	R^2	R^2 (modified)	The standard error of the estimate
Linear	0.808	0.654	0.651	0.427
Logarithmic	0.748	0.559	0.556	0.482
Inverse	0.675	0.456	0.452	0.535
Quadratic	0.873	0.762	0.759	0.355
Cubic	0.875	0.766	0.761	0.353
Compound	0.794	0.631	0.628	0.055
Power	0.727	0.529	0.526	0.062
S	0.651	0.423	0.419	0.068
Growth	0.794	0.631	0.628	0.055
Exponential	0.794	0.631	0.628	0.055
Logistic	0.794	0.631	0.628	0.055

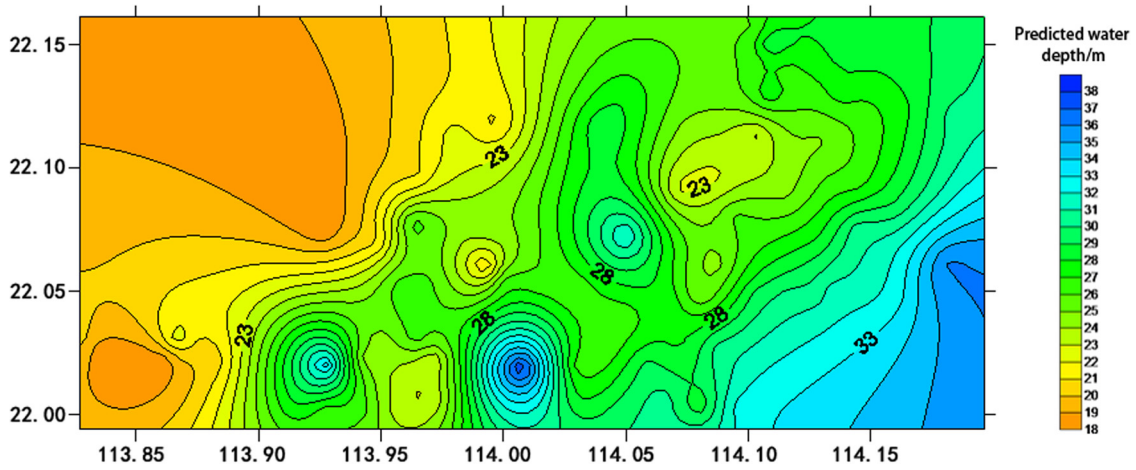

Figure 5: Prediction results of the water depth based on curve fitting models.

total data and 40% of the total data. The B1–B4 and B4/B1 band data were used as the input of the model.

The MAE of training results was 2.046, and the standard deviation was 2.621; the MAE of test results was 2.451, and the standard deviation was 3.228. The importance of predictive variables of the model was 0.28, 0.27, 0.23, 0.17, and 0.04 (B4/B1, B1, B2, B3, and B4, respectively). The inversion result is shown in Figure 10.

5 Comparative analysis and discussion

To better reflect the accuracy of each model, for each water depth inversion algorithm, the MAE between the inversion value of all prediction points and the measured value was calculated, and the results are presented in Table 4. Besides, for each model, the measured water

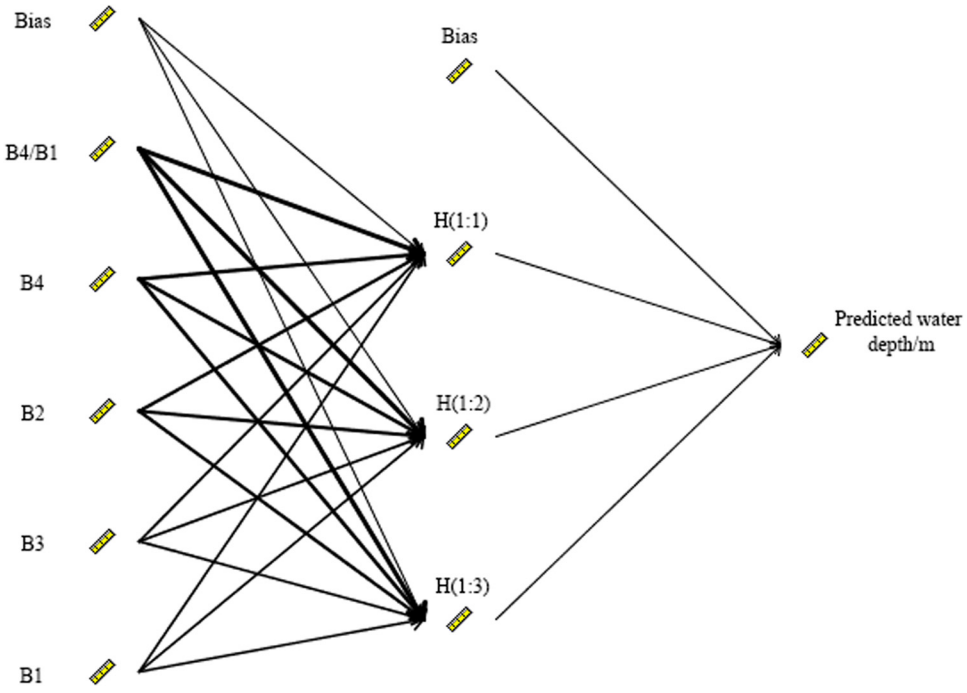

Figure 6: BP neural network structure.

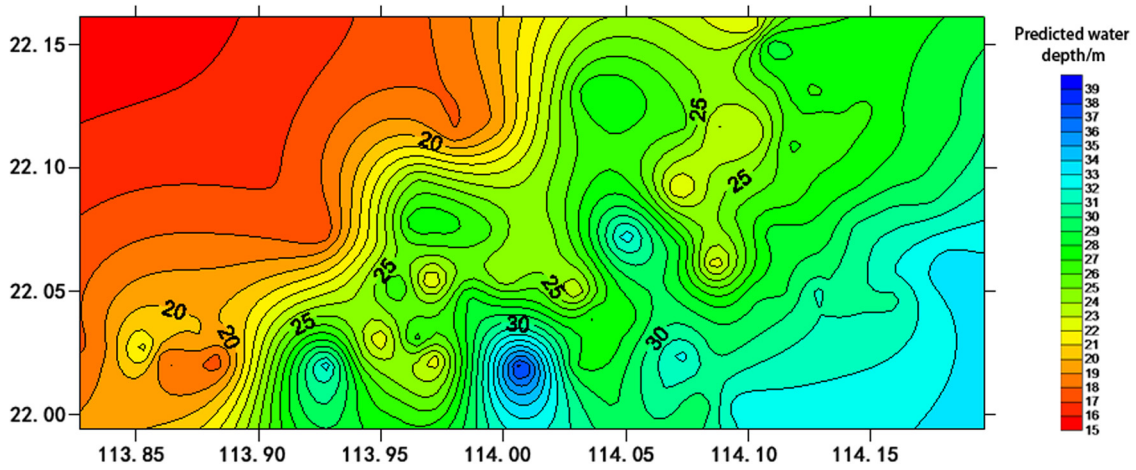

Figure 7: Prediction results of water depth based on the BP neural network.

depth value was taken as the horizontal axis of the plane rectangular coordinate system, and the inversion value was taken as the vertical axis of the coordinate system. All points were plotted in the coordinate system to get the error between the inversion value and the measured value, as shown in Figure 11.

The performance of several depth inversion algorithms is compared in Table 4. Table 4 indicates that

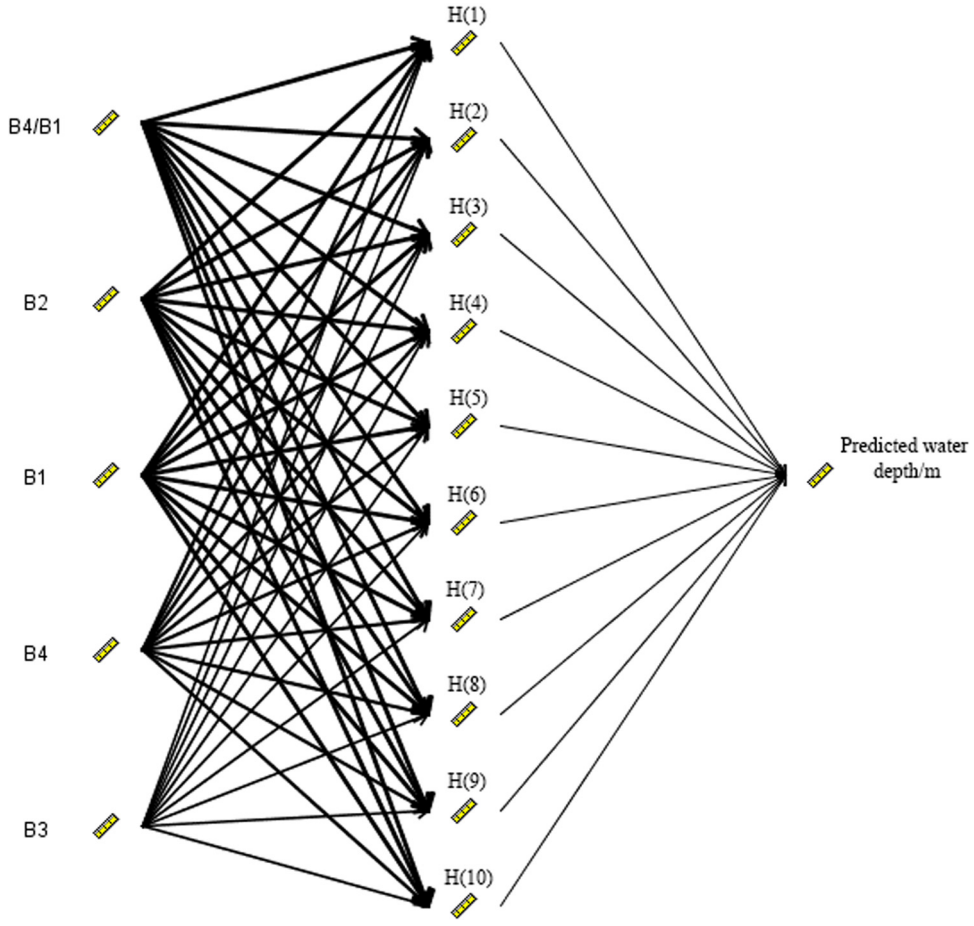

Figure 8: Structure of RBF neural network.

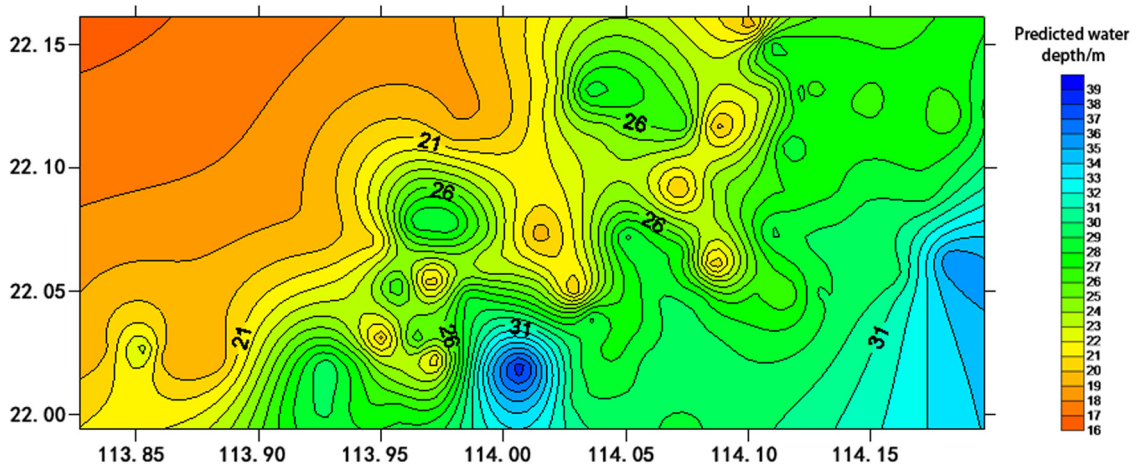

Figure 9: Prediction results of water depth based on the RBF neural network.

the MAE between the depth learning model and the measured water depth was the smallest (2.350 m), followed by the linear SVM model (2.451 m), and the BP neural network model was in the middle (2.455 m), and the errors of the curve fitting model and RBF neural network model were relatively large (2.575 m and 2.719 m, respectively). Therefore, the deep learning model was the best, followed by the linear SVM model and the BP neural network model, and the curve fitting model and RBF neural network model were poor.

Figure 11 directly reflected the deviation between the predicted water depth and the measured water depth at each inspection point. For the convenience of observation, the straight line passing through the coordinate origin, and slope of 1 was called "coincidence line" [17]. The inversion value of all inspection points on the coincidence line was equal to the measured value. The performance of several depth inversion algorithms was analyzed and compared from Figure 11.

From the curve fitting model in Figure 11(a), the distribution of prediction points was relatively scattered as a whole. When the actual water depth was less than 25 m, the prediction value of the model was generally greater than the measured value, and the fitting between the prediction point and the coincidence line was not good as a whole.

It can be seen from Figure 11(b) that for the BP neural network model, when the actual water depth value of the predicted point was greater than 35 m, the prediction error of the model was larger. When the actual water depth was about 30 m, the prediction accuracy of the model was higher. The upper prediction point fitted well with the coincidence line.

According to Figure 11(c), in the RBF neural network model, the overall distribution of prediction points was

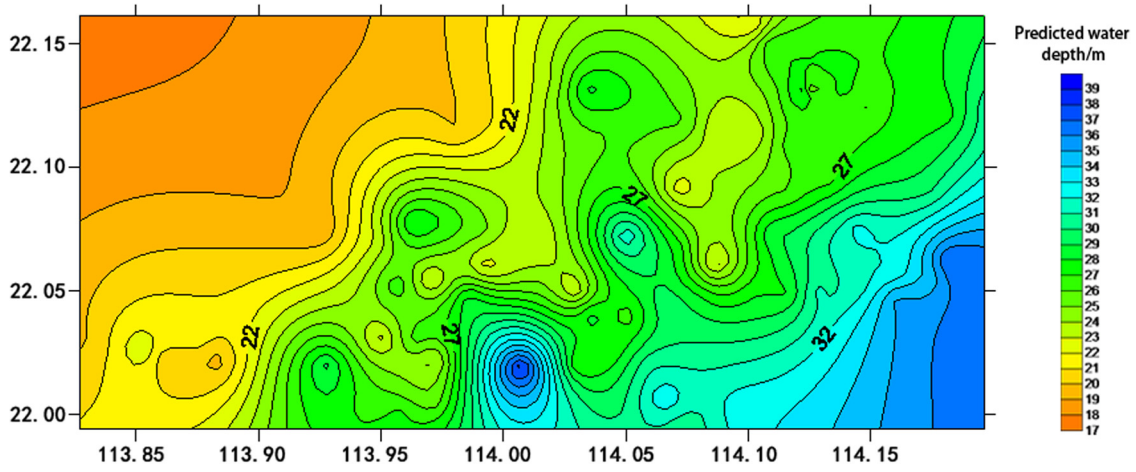

Figure 10: Water depth prediction results based on linear SVM.

Table 4: The MAE of five water depth inversion models

Model	MAE
Curve fitting	2.575
BP neural network	2.455
RBF neural network	2.719
Linear SVM	2.451
Deep learning	2.350

more centralized than that of the linear fitting model. Still, it was more decentralized than that of the BP neural network model. Although all prediction points were evenly distributed on both sides of the coincidence line, the error between them and the measured value was large, and on the whole, the prediction points and the coincidence line were not well fitted.

By using the linear SVM model in Figure 11(d), it turned that the distribution of prediction points was very similar to that of the BP neural network model, but

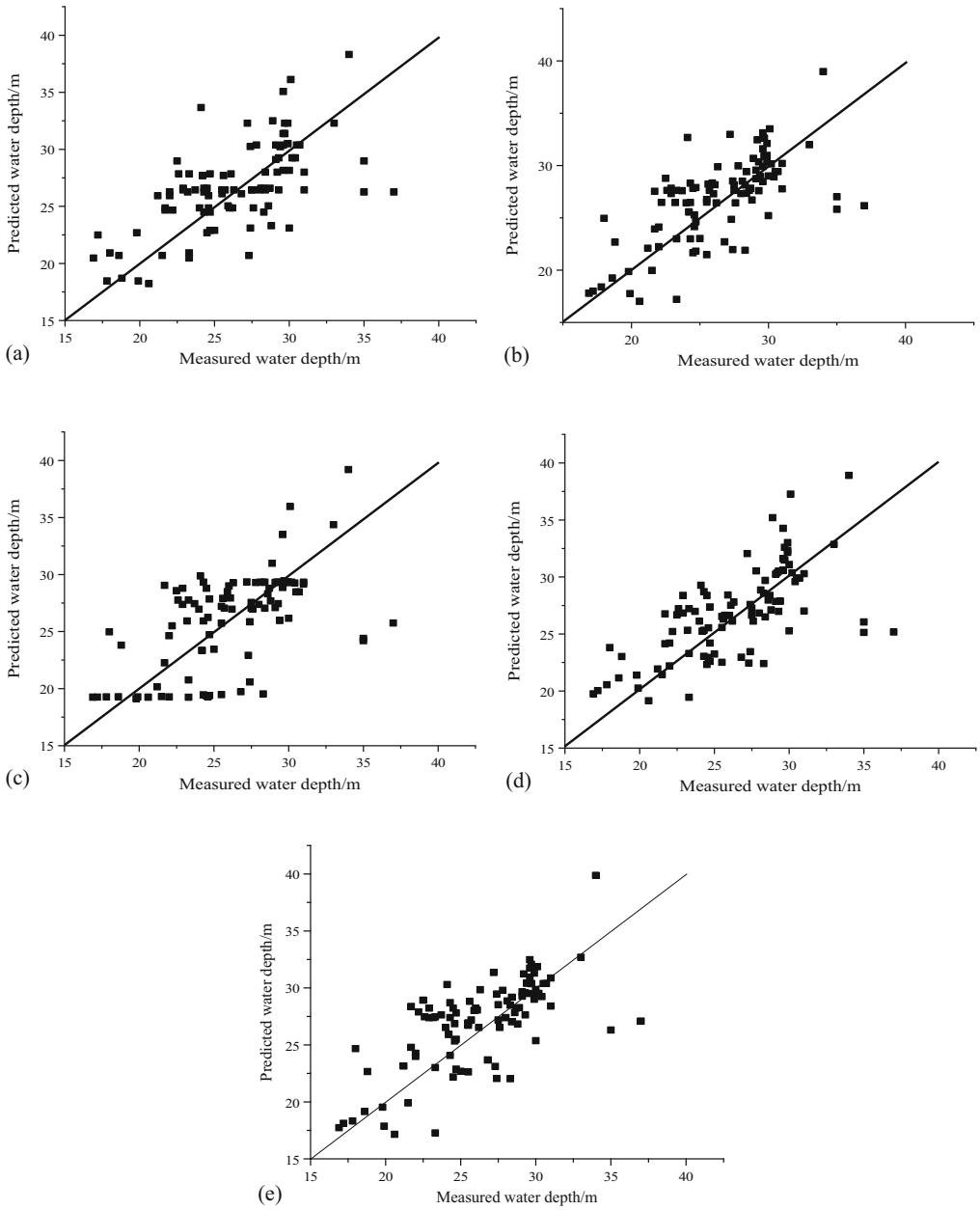

Figure 11: Deviation diagram of predicted and measured values of model water depth: (a) curve fitting model, (b) BP neural network model, (c) RBF neural network model, (d) linear SVM model, and (e) deep learning model.

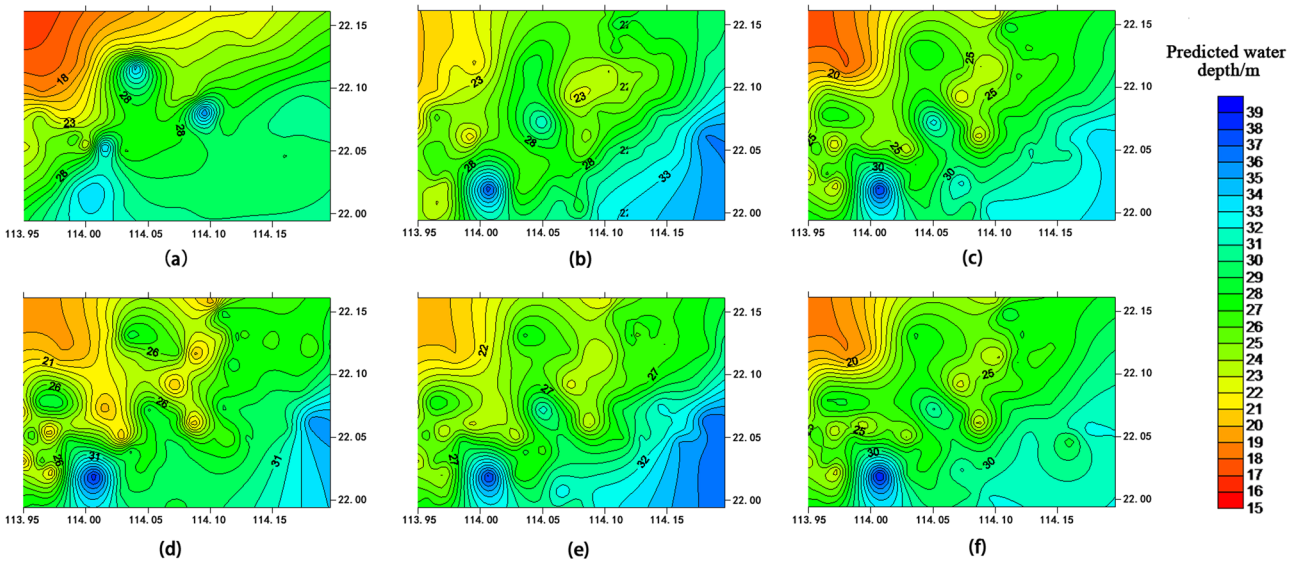

Figure 12: Inversion results of water depth in the study area: (a) actual water depth, (b) curve fitting inversion, (c) BP neural network, (d) RBF neural network, (e) linear SVM, and (f) deep learning inversion.

the dispersion degree of prediction points when the measured water depth about 30 m was greater than that of the BP neural network model. In addition, when the water depth was less than 23 m, the predicted value of water depth at the prediction point was generally greater than the measured value, and the fitting between the prediction point and the coincidence line was general.

Through the deep learning model in Figure 11(e), it can be learned that the distribution of prediction points was dense, but when the actual water depth value was less than 23 m or greater than 33 m, the error of prediction points was larger. The distribution was very similar to that of the BP neural network model, and the prediction points and the coincidence line were generally better.

From Figure 12(a)–(f), it can be seen that the results obtained by the five water depth inversion models had certain errors compared with the actual results, but the overall error of the deep learning model and the BP

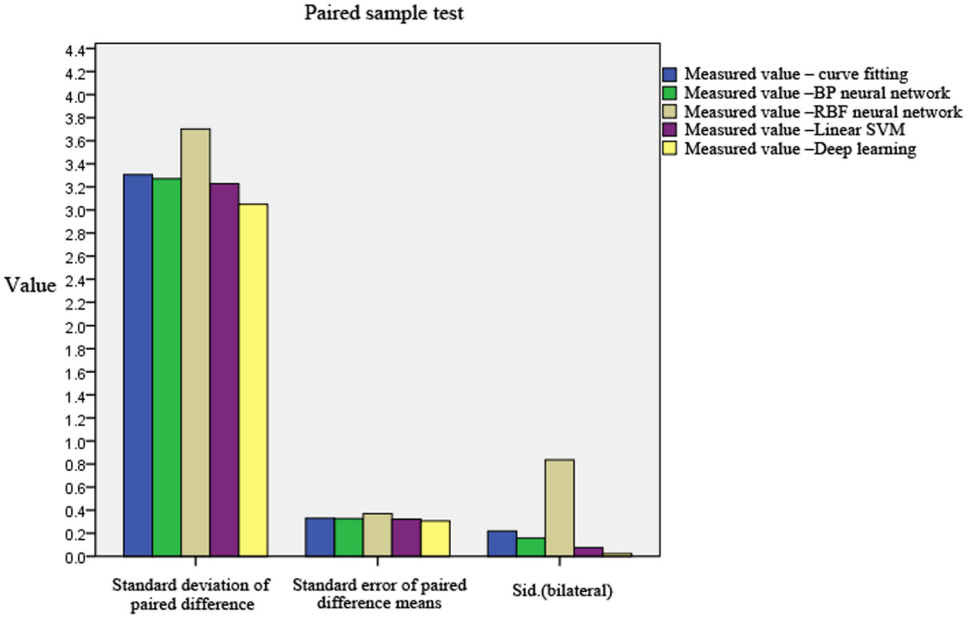

Figure 13: Comparison between inversion results of five models and measured values.

neural network model was smaller. The similarity of the actual result graph was higher, and the errors of the other three models were larger.

From the comparison of Figures 11(a)–(e), 12(a)–(f), and 13, it can be seen that the deep learning model had the best fitting degree, the BP neural network model took the second place, the linear SVM model was the third, and the RBF neural network and the curve fitting model were poor.

It can be seen that deep learning was better than the traditional machine learning algorithm in RS depth inversion. The reason was that the advanced features extracted from large amounts of data were unmatched by other simple algorithm. But the deep learning model often needs a large sample size to achieve the desired effect. Simple machine learning algorithm can also backpropagate the error through continuous transmission of water depth information, so as to adjust the error. Therefore, the accuracy of traditional machine learning algorithm was higher than that of the curve fitting model.

6 Conclusion

Based on the HJ-1B satellite data and the measured water depth data in the sea area near the islands outside the Pearl River Estuary, the water depth values of the sea area were inversed by various methods. Only from the curve fitting model, the cubic model was better than other curve fitting models. However, the error of machine learning method was less than that of the curve fitting method. Of course, the curve fitting method is simpler than the machine learning method, and there is no great requirement for the computer's computing power and machine configuration. Among the four machine learning methods, the deep learning model had the best inversion effect, followed by the BP neural network model. Therefore, the best method of this study was the deep learning model. As an advanced machine learning method, deep learning is a hot field of artificial intelligence, and its advantages in the image recognition field are far more than the previous technology. Although the RBF neural network was better than the BP neural network in generalization ability and learning speed, it was inferior to the BP neural network model in this study. The reason may be the adjustment of parameters such as the number of network layers, the number of nodes in each layer, the function type of nodes, and the epochs of the neural network model. The adjustment can achieve the best effect in the training, but cannot meet the requirements to achieve the best results in the test data. Therefore, to avoid under fitting and over fitting, the model parameters should be adjusted many times to select the most suitable model.

Acknowledgments: This research was supported by research and demonstration of ecological construction of typical islands in the South China Sea and the monitoring technology of ecological things in the South China Sea (Grant No. 2017YFC0506304); using remote sensing geology survey, the application information extraction and drawing of national defense construction (Grant No. DD2016007637); groundwater exploration technology in the water shortage region in '863' program (Grant No. 2012AA062601).

Conflict of interest: Authors state no conflict of interest.

References

[1] Yanjiao W, Wenjie D, Peiqun Z, Feng Y. Research progress on remote sensing methods for water depth and visible light. Mar Bull. 2007;26:92–101.
[2] Lian F, Chuanmin H, Xiaoling C, Xiaobin C, Liqiao T, Wenxia G. Assessment of inundation changes of Poyang Lake using MODIS obscrvations between 2000 and 2010. Remote Sens Environ. 2012;121:80–92.
[3] Hongchen Z. Research on multi-level decision-making optical remote sensing water depth inversion based on WorldView2. Nanjing: Nanjing University; 2017. p. 12–5.
[4] Ping Z. Mathematical model of visible light remote sensing. Ocean Lakes. 1982;13:225–30.
[5] Lyzenga DR. Passive remote sensing techniques for mapping water depth and bottom features. Appl Opt. 1978;17:379–83.
[6] Lyzenga DR. Remote sensing of bottom reflectance and water attenuation parameters in shallow water using aircraft and Landsat data. Int J Remote Sens. 1981;2:71–82.
[7] Polcyn FC, Brown WL, Sattinger IJ. The measurement of water depth by remote sensing techniques. Mich Univ Ann Arbor Inst Sci Technol. 1970;1970:7–9.
[8] Benny AH, Dawson GJ. Satellite imagery as an aid to bathymetric charting in the Red Sea. Cartogr J. 1983;20:5–16.
[9] John M, Paredes, Robert ES. Water depth mapping from passive remote sensing data under a generalized ratio assumption. Appl Opt. 1983;22:1134–5.
[10] Jingjing W, Qingjiu T. Research on inversion method of shallow sea water depth and hyperspectral remote sensing in coastal zone. Geogr Sci. 2007;27:843–8.
[11] Gang L, Fan Y, Cheng C, Dongmei W, Wenguang L. Research on depth extraction technology of Hongze Lake based on landsat-8 remote sensing image. Beijing Survey Mapp. 2017;4:13–8.
[12] Benqing C, Yanming Y, Kai L. Retrieval of island shallow water depth from the GaoFen-1 multi-spectral imagery. J Trop Oceanogr. 2017;2:70–8.

[13] Ying Z, Dong Z, Yanjiao W, Yong X. Research on remote sensing method of water depth in sandy waters. J Oceanogr. 2008;1:51–8.
[14] Cracknell AP, Ibrahim M. Bathymetry studies on the coastal waters (Red Sea) of Jeddah, Saudi Arabia, using Shuttle MOMS-O1 data. Int J Remote Sens. 1988;9:1161–5.
[15] Ying Z, Yun Z, Dong Z, Yan Q. Remote sensing of water depth in the radiation sand ridges of the Southern Yellow Sea. Chin J Oceanogr. 2009;31:39–45.
[16] Wenqian H, Di W, Yang Y, Zhicheng L, Yangyang Z. Multi-spectral remote sensing water depth inversion in shallow waters. Mar Technol. 2013;32:43–6.
[17] Zhonghan H, Baishan X, Chenglin Y, Yongjin S. Research on reef depth retrieval of south China Sea Island based on planet multispectral image. Geomat Spat Inf Technol. 2020;43:139–142+146.
[18] Sandidge JC, Holyer RJ. Coastal bathymetry from hyperspectral observations of water radiance. Remote Sens Environ. 1998;65:341–52.
[19] Wang Y. Research on remote sensing method of water depth based on the impact of suspended sediment. Doctoral dissertation. Nanjing: Nanjing Normal University; 2010. p. 75–90.
[20] Zhicheng L, Wenqian H, Yang Y, Yangyang Z. Multi-factor remote sensing water depth inversion model based on neural network technology. Survey Mapp Eng. 2012;21:17–21.
[21] Hongqi S, Chunxia C, Long Y. Research on water depth inversion method of hyperspectral image based on SVR. N Industrial. 2014;1:75–8.
[22] Xu L. Multi-factor remote sensing water depth inversion based on neural network technology. Master degree thesis. Beijing: China University of Petroleum; 2014. p. 7–13.
[23] Yanguo F, Jinxia L. Research on remote sensing water depth inversion model based on neural network technology. Mar Survey Mapp. 2015;35:20–3.
[24] Bin C, Zhenge Q, Shulong Z, Bincai C. Improvement of BP neural network remote sensing water depth inversion algorithm. Bull Survey Mapp. 2017;2:40–4.
[25] Guizhou Z, Xiaodong L, Hongping W, Weihua H. Inversion of water depth from WorldView02 satellite imagery based on BP and RBF neural network. Earth Sci. 2017;12:2345–53.
[26] Chen X. Research on deep learning algorithm and application based on convolutional neural network. Zhejiang: Zhejiang Gongshang University; 2014.
[27] Tingxu D, Hongbo J, Chao C, Qiming Q. Inversion of shallow snow depth based on measured spectral analysis of HJ-1B data. Spectrosc Spectr Anal. 2011;31:2784–8.
[28] Runping S, Anqi H, Bolun L, Jia G. Construction of a drought monitoring model using deep learning based on multi-source remote sensing data. Int J Appl Earth Obs Geoinf. 2019;79:48–57.
[29] Haixiang L, Caiming Z, Xiuxia L. Conic fitting of scattered data points on a plane. J Comput Des Graph (Chin). 2004;16:1594–8.
[30] Xiaochuan W, Feng S, Lei Y, Yang L. MATLAB neural network 30 case analysis. Beijing: Beihang University Press; 2010.
[31] Bin C, Zhenge Q, Bincai C. Comparison of four remote sensing algorithms for shallow water depth inversion. J Geomat Sci Technol. 2016;33:388–93.
[32] Zhengdong D, Xin Y, Hongjun G, Dehao Y. Remote sensing of water depth based on RBF neural network. J PLA Univ Sci Technol (Nat Sci Ed). 2013;14:101–6.
[33] Jinshang Z, Xuanyu J, Zhenzhen S. Water depth inversion based on support vector machine and BP neural network. Geomat Spat Inf Technol. 2019;6:11–4.